

**Effect of charge transfer on EELS integrated cross sections in Mn and Ti oxides**

Pavel L. Potapov, Kevin Jorissen, and Dominique Schryvers  
*EMAT, University of Antwerp, Groenenborgerlaan 171, B-2020 Antwerp, Belgium*

Dirk Lamoen

*TSM, University of Antwerp, Groenenborgerlaan 171, B-2020 Antwerp, Belgium*

(Received 10 November 2003; revised manuscript received 16 March 2004; published 19 July 2004)

The influence of the charge transfer between metal and oxygen atoms on the EELS integrated cross sections has been studied experimentally and theoretically in titanium and manganese oxides of different valence. It is demonstrated that the behavior of the metal  $L_{2,3}$  integrated cross section can be connected with the formal valence of the compound. The charge depletion is most noticeable in the energy-loss region 10–20 eV above the threshold while, at greater energy windows, the increasing contribution of continuum states masks the effect of the charge transfer. This contribution of continuum states is independent of the local chemical environment and can be calculated in a free atom model. Complementary, the integrated cross section near the threshold can be reliably calculated by the LAPW method provided that the simulation of EELS accounts for the matrix elements and angular dependence of the scattering. The LAPW method is successful near the threshold, however, at higher energy-losses, the standard LAPW basis set is insufficient with respect to the continuum states. Extending the basis set with extra localized orbitals allows one to account partially for the contribution of the continuum states and therefore to enlarge the applicability range of the LAPW calculations. The created core hole might noticeably affect the intensity scale of integrated cross sections but this can be modeled by introducing a core-hole in calculations also. Finally it is demonstrated that the effect of charge transfer on EELS cross sections is adequately reproduced by the LAPW calculations.

DOI: 10.1103/PhysRevB.70.045106

PACS number(s): 79.20.Uv, 34.80.-i, 82.80.Pv

**I. INTRODUCTION**

The bonding trends in the formation of a compound from pure elements can be understood in terms of the redistribution of the electron density. Namely, the energy distribution of the density of states (DOS) around each atom changes and some portion of the electron charge can be transferred from one atom to another. The information about the unoccupied DOS is readily accessed by analyzing the fine features in electron energy loss spectra (EELS) or x-ray absorption spectra (XAS). However, it is more difficult to establish a clear connection between the charge transfer and the EELS or XAS in different compounds. Theoretical considerations suggest that the charge transfer might affect the integrated area of EELS or XAS cross sections but the effect is hard to measure experimentally. In the present work, the charge transfer effect will be considered with respect to EELS ionization edges although all major conclusions should also be relevant for XAS.

The measurement of absolute EELS integrated cross sections is not practical as the total signal depends on numerous experimental parameters such as the beam current, probe size, and specimen thickness. Only relative changes in the cross section are commonly measured based on the fact that the scattering on a given atom becomes less dependent on its local chemical environment with increasing energy-loss.<sup>1–5</sup> In this approach, the EELS near-edge cross section is normalized to a scattering level far above the threshold. However, the precision of such measurements is in most cases insufficient because the normalization window should be chosen at high enough energy-loss where the errors arising

from imperfect background subtraction and the effect of plural scattering become significant. As a result, experimental studies typically report changes in the EELS cross sections close to the error bar and the overall effect of the charge transfer on EELS is questionable. In a few rare cases, the charge transfer can be visualized in the appearance of new features at EELS edges. The classic example is the absence of the white line in metallic Cu while this line appears in CuO oxide due to the partial emptying of the Cu  $d$ -band.<sup>6</sup> Even in this (rare) case, the presence of the charge transfer can be doubted as the sharp white line in principle might be formed by the fusion of a few broad peaks present at the edge of metallic Cu.<sup>5</sup>

The effect of the charge transfer on the integral cross sections is essential for elemental analysis of compounds with EELS. Suppose, for instance, that a metal Me forms an oxide  $\text{Me}_x\text{O}_y$ . The composition can be measured by relating the integrated intensities  $I_{\text{Me}}$  and  $I_{\text{O}}$  of two EELS edges:

$$\frac{I_{\text{Me}}(\Delta E)}{I_{\text{O}}(\Delta E)} = \frac{x \sigma_{\text{Me}}(\Delta E)}{y \sigma_{\text{O}}(\Delta E)}, \quad (1)$$

where  $\Delta E$  is an energy window in which the integration is performed and  $\sigma_{\text{Me}}$  and  $\sigma_{\text{O}}$  are the cross sections of Me and O atoms, which are supposed to be constants. The question is how significantly the valence state of a Me atom could affect its cross section  $\sigma_{\text{Me}}$ ?

In the present paper, the influence of the charge transfer on EELS integrated cross sections is measured experimentally and compared with theoretical predictions in the series of Ti and Mn oxides. In order to avoid complication from the

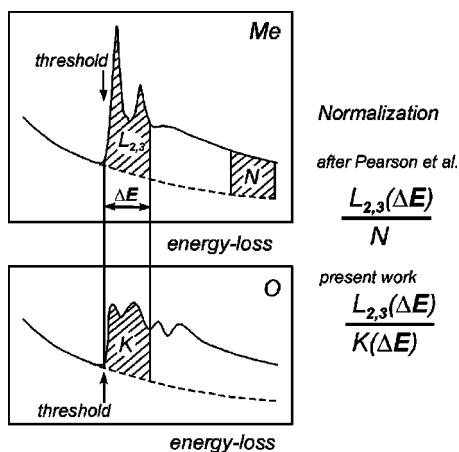


FIG. 1. Comparison of the normalization method after Pearson *et al.* (Ref. 1) with the method employed for normalization of  $L_{2,3}$  edge counts in the present work.

orientation dependence of scattering, both experimental and theoretical spectra are averaged over random crystal orientations. In the experiment, the focus is on a comparison between the cross sections in oxides of different valence, namely II and IV valence oxides. Instead of using the high energy-loss normalization window,<sup>1</sup> the experimental metal  $L_{2,3}$  integrated intensity is divided to the O  $K$  one in the same energy window near the threshold. In other words, we deduce directly the  $I_{Me}/I_O$  value, thus errors from background and plural scattering are minimized. The difference between these two normalization methods is outlined schematically in Fig. 1. Provided that two edges are recorded from the same place and with the same beam intensity and the composition of the oxides is exactly known, the cross sections ratio can be precisely deduced. For very small windows our normalization procedure might result in oscillation of the Me cross section due to the fine structure of the O  $K$  edges, however, this oscillation quickly damps out with increasing window width.

The calculation of the integrated cross section for analytical purpose is conventionally performed within an atomic model,<sup>7,8</sup> which apparently cannot account for the charge transfer. The charge redistribution is readily accessible in *ab initio* band structure methods, which have been applied for calculating the energy-loss near edge structure (ELNES). Although the relative intensities of different ELNES features are reproducible by these methods, the comparison of integrated cross sections in different compounds is not secure, as the resulted intensity scale is arbitrary. However recent developments in the calculation of the EELS dynamic form factor accounting explicitly for the matrix elements and angular dependence of scattering<sup>9,10</sup> in principle allow one to put the calculated cross section of different materials on the same intensity scale. In the present work, the *ab initio* linearized augmented plane waves (LAPW) method is used and demonstrated to reproduce reliably the EELS integrated cross sections. In the Appendix it is shown that the internal computational parameters in LAPW when chosen in a reasonable range do not significantly affect the calculated EELS cross section for a given compound. Special attention is paid

to the energy range of applicability of the LAPW method and the reasons why it is less reliable at high energy-losses where the simpler atomic calculations work better.

## II. DETAILS OF CALCULATIONS AND EXPERIMENT

### A. Experiment

Both investigated oxide series consist of at least two oxides of different valence. For quantification purposes the composition of each oxide must be exactly known. The IV valence  $MnO_2$  and  $TiO_2$  oxides—rutile and anatase—and also the II valence  $MnO$  oxide perfectly satisfy these criteria. In the case of II valence  $TiO$  oxide, the situation appears to be more complicated. This oxide (NaCl-type structure) might exhibit a noticeable deviation from the 50:50 composition in both directions due to vacancies at the titanium or oxygen sites.<sup>11,12</sup> According to Andersson,<sup>11</sup> the oxygen content in  $TiO$  correlates linearly with the lattice parameter. In our case, the cubic lattice parameter was measured by x-ray diffraction to be 0.472 nm, which corresponds to a composition of  $TiO_{1.2}$ .<sup>11</sup>

A Philips CM30 transmission electron microscope operating at 297 kV and equipped with a GIF200 for EELS analysis was employed. In order to avoid the influence of channeling the orientation of each crystal was kept away from any exact zone orientation. The spectra were observed in diffraction mode with collection and convergence angles equal to 3.75 and 2.2 mrad, respectively. The energy resolution was 1.2 eV. The probe size varied from 10 to 30 nm and the typical acquisition time was 5 s. The good reproducibility of fine features in EELS suggests that the beam damage was minor in all cases. For each spectrum, the low-loss spectra were automatically acquired before and after the characteristic high-loss one with a minimal pause among acquisitions ensuring that the probed region remains the same. In the cases when the probe was contaminated or the sample was drifting in the course of acquisitions, the initial and final low-loss spectra differed from each other and the whole measurement was discarded.

The background was removed by extrapolation of the pre-edge region to the higher energies as a power-law. The procedure is not quite reliable when two edges partially overlap as in the case of O  $K$  and Ti  $L_{2,3}$  edges in titanium oxides. To extract accurately the oxygen count it is additionally assumed that the profile of the Ti edge at high energies follows closely the free-atom scattering curve. As will be demonstrated in Sec. III B, this assumption is valid for energy-losses higher than 70 eV above the Ti threshold and therefore is accurate in the region of the O  $K$  edge. The plural scattering was removed by Fourier-ratio deconvolution<sup>13</sup> with the low energy-loss spectrum obtained from exactly the same region in the sample, as described above.

### B. Calculations

Band structure calculations were performed using the full-potential linearized augmented plane wave code WIEN2K (Ref. 14) with the generalized gradient approximation (GGA) for the exchange-correlation functional. The code is

based on density functional theory (DFT) and uses a mixed basis set consisting of linearized augmented plane waves (LAPW) and augmented plane waves plus local orbitals (APW+lo). The APW+lo set uses fixed energies for radial basis-functions and resembles LAPW rather than the old Slater APW approach, so, for brevity, we will further call the method LAPW. EELS was calculated by determining the dynamic form factor in the first Born approximation and integrating it over the momentum transfer to take the collection and convergence angles into account in the formalism described by Nelhiebel *et al.*<sup>9</sup> and Hébert *et al.*<sup>10</sup> No orientation dependence of EELS was considered, i.e., the cross sections were averaged over all possible directions of the scattering vector with respect to the crystal.

MnO<sub>2</sub>, TiO<sub>2</sub> rutile and anatase exhibit a tetragonal lattice ( $c/a < 1$  for MnO<sub>2</sub> and rutile and  $c/a > 1$  for anatase). The NaCl-type lattice was adopted for both MnO and TiO<sub>1.2</sub>. Although in reality the latter possesses vacancies at Ti sites, the perfect TiO-structure was used in the calculations assuming that the chemical environment for O atoms only changes negligibly comparing with the ideal NaCl-type lattice. For calculating the EELS of pure metals and intermetallics, the modifications with the simplest lattice were chosen, namely, fcc for Mn, hcp for Ti, CsCl-type for NiMn and TiNi. All lattice parameters were optimized to achieve minimal forces at the atoms, except for the case of Mn metal and MnO<sub>2</sub> oxide. In the latter materials, optimization yielded cross sections inconsistent with experiment, possibly because magnetic effects were not considered in the present work. Thus, the experimental lattice parameter for MnO<sub>2</sub> and for high temperature paramagnetic fcc Mn was taken without optimization.

For Mn and Ti the 1s, 2s, and 2p states, for Ni 1s, 2s, 2p, and 3s, and for O the 1s state were considered as core electron states and calculated self-consistently, fully relativistically and numerically in the spherically averaged crystal potential. The basis cutoff  $RK_{\max}$  (i.e., the product of the smallest muffin tin radius in the system and the length of the maximum  $\mathbf{k}$ -vector of the interstitial plane wave basis) was typically 7–8. The converged  $\mathbf{k}$ -meshes consisted of 1000–2000  $\mathbf{k}$ -points in the full Brillouin zone. Core hole calculations were performed in supercells consisting of  $2 \times 2 \times 2$  simple unit cells, containing 64 atoms in the case of MnO and TiO, and 48 atoms for MnO<sub>2</sub> and rutile TiO<sub>2</sub>. Evidently, smaller  $\mathbf{k}$ -meshes were used for core hole calculations.

The atomic calculations were performed by the standard routine using the Gatan EL/P software. The Hartree-Slater cross sections were calculated based on the tabulation of generalized oscillator strength following the approach of Leapman *et al.*<sup>7</sup> and Ahn *et al.*<sup>8</sup> Account for the finite collection angle was made after Egerton<sup>13</sup> and for convergence angle after Kohl.<sup>15</sup>

### III. RESULTS

#### A. Extracting experimental cross sections: Evidence of charge transfer

Figure 2 shows the experimental EELS of several Mn and Ti oxides with different valence. Each compound exhibits its

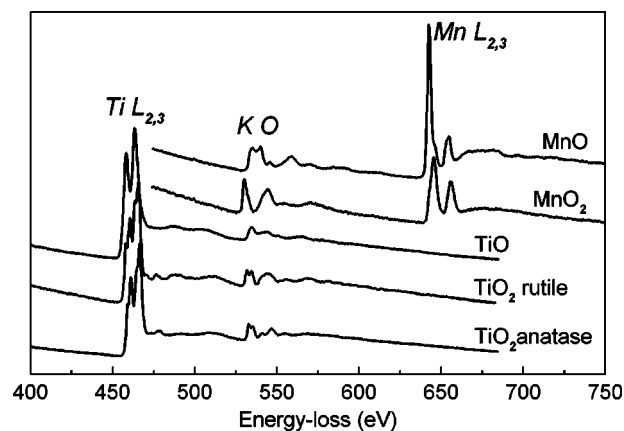


FIG. 2. Overview of the experimental EELS in the examined oxides.

own specific energy-loss near-edge structure (ELNES) and slightly varying onset position. In the present work we will, however, focus on the edge area integrated over a certain energy window. Provided that the one-event ionization counts are accurately isolated from the background and stripped off plural scattering, the integrated area yields information about the number of atoms in the probe and their EELS scattering cross section. The latter relates with the number of empty states in the valence bands available for transition. Due to the transition selection rule (which our calculations suggest to be valid for the examined materials and present experimental conditions) these are  $p$ -like for the  $K$  edge and  $d$ -like for the  $L_{2,3}$  one. Since the atomic ratio between metal and oxygen is exactly known for each oxide, the experimental ratio between the metal  $L_{2,3}$  and oxygen  $K$  cross sections can be deduced in any energy window. If the charge transfer effect on EELS is negligible, the metal  $L_{2,3}$  cross sections normalized on the O  $K$  ones are supposed to be the same for oxides of different valence. However, if the concept of charge transfer is relevant in EELS, the normalized metal  $L_{2,3}$  cross sections should change when going from the II valence to the IV valence oxide. Namely, a smaller charge around a metal atom in the IV valence oxide would imply the deficiency of electrons in the conduction band and therefore a higher number of empty states available for the transitions, i.e., a higher EELS cross section. The O  $K$  cross section in such a simple intuitive picture should not vary as the excess charge in the IV valence oxide is distributed over the double amount of oxygen atoms.

Table I lists the experimental Mn and Ti  $L_{2,3}$  cross sections integrated in different energy windows and normalized on the O  $K$  ones taken in the same windows. In all cases, the metal  $L_{2,3}$  cross sections are smaller in II valence oxides than in IV valence ones, which is consistent with the expectation of the charge transfer. The difference is most pronounced for the 20 eV window and decreases with increasing energy window. At the same time, the Ti oxides of IV valence, rutile and anatase, show almost identical cross sections in all energy windows.

These data correlate with the previous results of Kurata and Colliex,<sup>2</sup> who reported an about 60% increase of the MnO<sub>2</sub> cross section with respect to MnO. They interpolated

TABLE I. Experimental Mn and Ti  $L_{2,3}$  cross sections normalized on the O  $K$  ones. The cross sections are extracted from the edge intensities and accounting for the nominal stoichiometry of an oxide.

Energy window (eV)	(Mn $L_{2,3}$ )/(O $K$ ) cross section		(Ti $L_{2,3}$ )/(O $K$ ) cross section		
	MnO	MnO <sub>2</sub>	TiO <sub>2</sub>		
			TiO	Rutile	Anatase
20	2.44	3.16	7.28	9.28	9.08
40	2.02	2.31	5.26	6.26	6.10
70	1.96	2.00	4.36	4.96	4.78

the white lines by a Lorentzian curve and normalized to the continuum following Pearson's method. However, the normalization method employed in the present work suggests rather a 30% increase of the MnO<sub>2</sub> cross section in the 20 eV window, which captures the region of the white lines. The difference is believed to come from the reduced errors in background subtraction and plural scattering deconvolution when the improved normalization method is used (see Introduction). In the following sections, it will be shown that our numbers agree much better with the LAPW calculations than the numbers reported by Kurata and Colliex.<sup>2</sup>

### B. LAPW vs atomic calculations of EELS cross sections

LAPW calculations typically work well only in a limited range of the energy-loss. The situation is illustrated by Fig. 3, where the experimental profiles of Ti and Ni  $L_{2,3}$  and O  $K$  edges are plotted together with those calculated by LAPW and a free-atom model. The energy broadening of the LAPW calculated profiles are fitted to match closely the width of peaks observed in the experimental curves. In such comparisons, the absolute intensity scale is arbitrary but analyzing the ELNES profile suggests that LAPW fits experiment accurately near the edge threshold while it tends to progressively underestimate the scattering intensity with increasing energy. Essentially this LAPW trend is independent of the chosen compound. Complementary, the simpler model of a free atom, which assumes scattering from the localized inner shell into the continuum states works well at high energies but of course fails to reproduce the EELS profile near the edge threshold.

In both the LAPW and atomic methods, the integrated cross section is calculated in the first Born approximation and within the one-electron picture yielding

$$\sigma = \frac{4\gamma^2 k}{a_0^2 k_0} \int \frac{1}{q^4} \sum_{i,f} |\langle f | e^{i\mathbf{q}\cdot\mathbf{r}} | i \rangle|^2 d\Omega, \quad (2)$$

where  $i$  stands for initial core,  $f$  for all available final states;  $\mathbf{k}_0$  and  $\mathbf{k}$  are initial and final wave vectors of the incident electron while  $\mathbf{q}$  is their difference, called the scattering vector;  $\Omega$  is the solid angle,  $a_0$  is the Bohr radius, and  $\gamma$  is a relativistic factor. As the initial core wave functions entering the formula (2) are insensitive to the chemical environment,

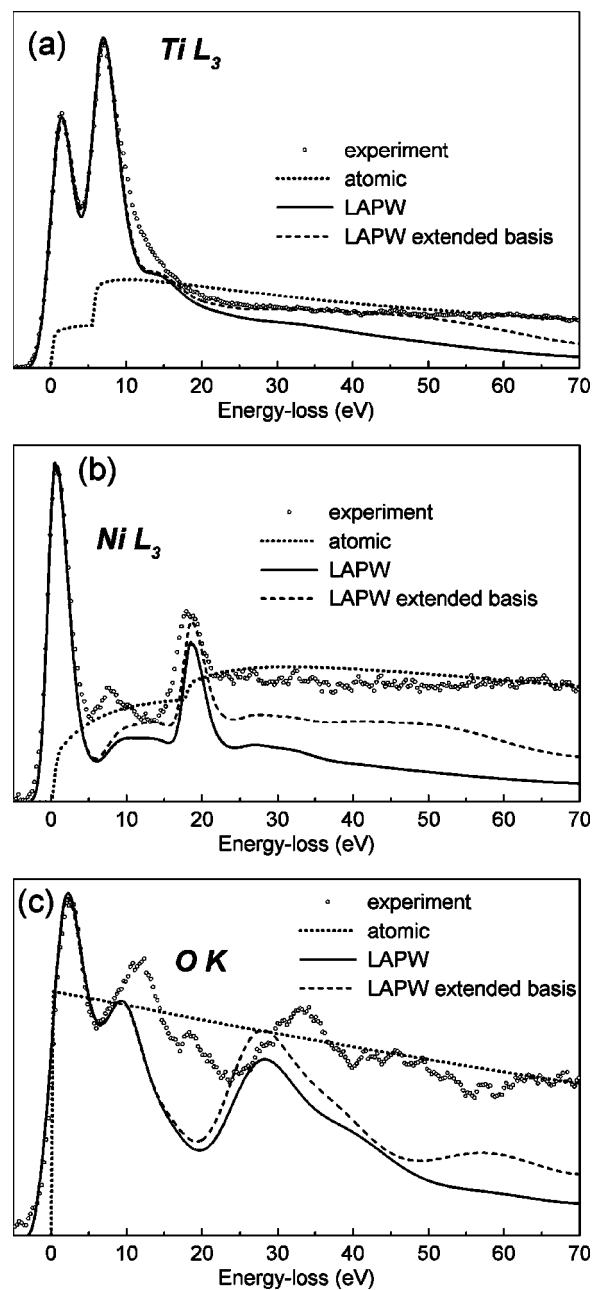


FIG. 3. Experimental, LAPW and atomic calculated EELS of (a) Ti  $L_{2,3}$  and (b) Ni  $L_{2,3}$  edges in TiNi and (c) O  $K$  edge in TiO. In (a) and (b), the experimental  $L_3/L_2$  branching ratio was introduced empirically into both LAPW and atomic calculations. The LAPW curves are broadened with energy-dependent broadening parameters (Ref. 16).

all the changes in cross sections relate solely to changing the final valence states.

In atomic calculations,<sup>7,8</sup> the final states are assumed to be continuum states, i.e., states found by solving the radial Schrödinger equation for a free atom with the positive eigenenergies falling into the continuum range. The effective potential in this case can be represented as a Coulomb central field, thus no self-consistent calculations are needed. Greatly simplifying the computation, the atomic approach does not take the band structure into account leading to a significant

deviation from experiment in the case of sharp bands like a  $d$ -band in transition metals.

In LAPW methods, the states are projected on the wavefunction basis set consisting of plane waves in the interstitial region between the atoms, augmented by radial functions times spherical harmonics inside muffin tin spheres (MT). These radial functions are solutions to the radial Schrödinger equation at a fixed energy. Self-consistent solution of the Kohn-Sham equations yields the ground state density of electrons and allows one to calculate unoccupied Kohn-Sham states. As DFT is a ground state theory, strictly speaking these states do not correspond to elementary excitations of the real system. However, using Kohn-Sham states as final states in formula (2) is usually a good approximation when assuming that the self-energy of excitations varies slowly in the considered energy range.<sup>3</sup> More importantly, there is a practical limitation of LAPW methods for calculating the high-energy states as the standard LAPW basis set is chosen to be economic, i.e., combining the accurate description of the crystal potential with reasonable computing time. In the case of LAPW, the set is constructed by linearization scheme, which employs derivatives around some reference eigenenergy usually taken in the center of the valence/conduction band. Reproducing accurately the occupied electronic states in the band and therefore calculating well the crystal potential, LAPW can cause a noticeable deviation from the exact solution for energies far above the Fermi level. The systematic underestimation of the scattering level at high energy suggests that the basis set is indeed insufficient in this region, i.e., there are states that are orthogonal to all the basis wave functions and that are missing in the calculations. At the same time, the success of atomic calculations in the same region indicates that the missing states have primarily a continuumlike character.

The impact of the insufficiency of the LAPW basis set on the simulated EELS spectra in each specific case depends on the ratio between the bound and continuum states. The Ti  $L_{2,3}$  edge [Fig. 3(a)] is dominated by the strong contribution of the unoccupied  $d$ -band, thus missing some of continuum states is not strongly noticed. In the case of Ni  $L_{2,3}$  edge [Fig. 3(b)], the  $d$ -band is almost filled, thus the contributions from the bound and continuum states are comparable and missing a major portion of the latter is important. In the O  $K$  edge [Fig. 3(c)], the bound states are associated with the  $2p$  band having little holes and the contribution of continuum states is again significant.

In an attempt to improve the applicability of the LAPW methods for the high energy final states, we extended the standard basis set. Namely, additional localized orbitals were introduced in the energy region of 30 eV above the Fermi level. The introduced additional basis functions tend to improve the fit with the experiment confirming our suggestion about the insufficiency of the standard basis set at high energies. With the new extended basis set, the Ti  $L_{2,3}$  edge was described nearly perfectly up to the energy of 50 eV, as seen in Fig. 3(a). In the case of Ni  $L_{2,3}$  and O  $K$  edges [Figs. 3(b) and 3(c)], the description of EELS spectra is noticeably improved although some of the continuum states seem to be still missing. Unfortunately, the possibilities of adding localized orbitals are currently limited in the LAPW implementa-

tion that we used, preventing a more systematic investigation. It might look surprising that introducing local orbitals describes well the contribution of continuum states in EELS despite the fact that these orbitals are localized inside the MT spheres and do not resemble the shape of delocalized continuum states. However, only the part of continuum wave functions within the MT spheres is important for EELS, while the part leaking out from the spheres is described by interstitial plane waves and does not directly influence the EELS cross sections, since it does not overlap with the core orbitals.

### C. Extended-basis LAPW calculations of EELS cross sections

Figures 4(a) and 4(b) show the calculated spectra (aligned to the threshold) in examined Mn and Ti oxides together with the spectra of pure metals and some intermetallic compounds. In all cases, the ELNES near the threshold shows the fine features characteristic to each material. However, the integration of the cross section in windows greater than 5–10 eV washes out the individual peaks and reveals general trends independent of the specific shape of ELNES. Figures 4(c) and 4(d) show the integrated cross sections as a function of the energy window as started from the threshold. To track better the trends in changing cross sections, the  $L_3$  edge is not superposed with the  $L_2$  one. Similar to experiment, the  $L_3$  cross sections in the IV valence oxides are always higher than those in the II valence oxides. The effect is clearly seen in the 10–15 eV windows and the difference between cross sections is stabilized as of 15 eV. Beyond 15 eV, all integrated cross sections grow proportionally although some small oscillations around the mean are visible.

It is further noted that the integrated cross sections of rutile and anatase are almost the same indicating that their behavior relates mainly with the valence IV of the TiO<sub>2</sub> oxides but not with their particular ELNES. On the other hand, the difference between cross sections of metals (pure or intermetallic) and II valence oxides is minor again confirming the relationship between the formal valence and the integrated cross section.

As seen from Figs. 5(a) and 5(b) the ELNES of O  $K$  edge is much more extended than that in the  $L_3$  one due to the larger width of the oxygen  $2p$  band. The corresponding cross sections [Figs. 5(c) and 5(d)] show the local oscillations, which are expected to get washed out when applying the energy-dependent broadening as we did ad hoc in Fig. 3(c) to mimic lifetime effects. Neglecting these oscillations, the cross sections increase almost linearly from the start to the entire energy-window range [Figs. 5(c) and 5(d)], which justifies the procedure of normalization on the O  $K$  cross section used in Sec. III A. Note that, on average, the integrated O  $K$  cross section in IV valence oxides seems to stay slightly below than that in II valence ones. This may indicate a slight increase of the electron charge around the oxygen atom in oxides of higher valence, which goes beyond the intuitive picture described in Sec. III A.

### D. Influence of core hole

The calculations described in the previous chapter were done in the sudden approximation, i.e., considering the

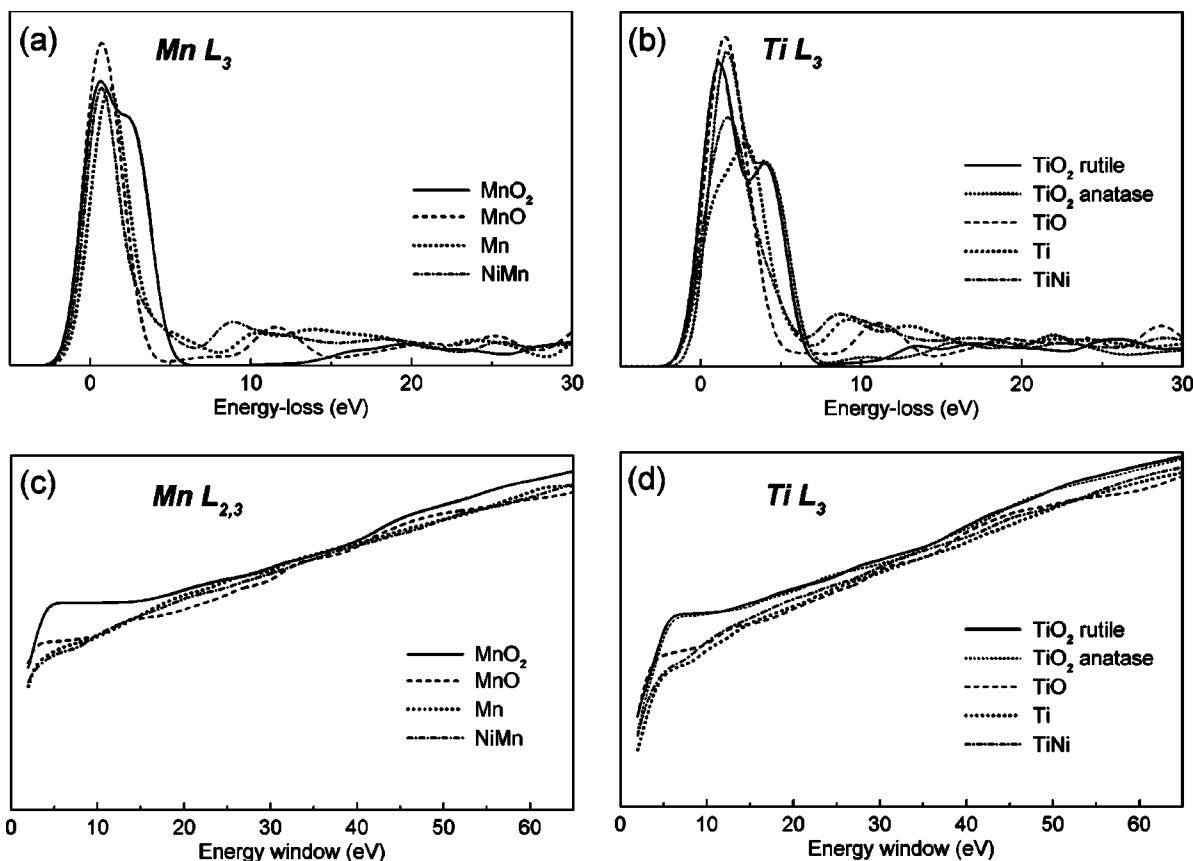


FIG. 4. LAPW ground state calculated (a,b) ELNES and (c,d) integrated cross sections of the (a,c) Mn  $L_3$  and (b,d) Ti  $L_3$  edge in different materials.

ground state of the system. It has been pointed out that an EELS ionization event relates rather with the excited state, in which a hole at the core shell is created by the incident electron. As a response to the creation of the core hole the electron system relaxes causing redistribution of DOS and therefore changes in the ELNES. The DFT, employed in the present calculations, is essentially a ground state formalism, which is not exact for an excited state. Nevertheless, different approximations for treating the excited state as a quasi-stable one have been explored in the framework of DFT. The earliest, so-called “Z+1 approximation,” replaced the scattering atom for the next one in the periodic table partially imitating the compression of the electron orbitals due to the core hole but neglecting the difference between, e.g., a core hole in the  $K$  and  $L$  shells. A more sophisticated approach directly introduces the frozen hole in the inner orbital and puts the excess charge as an extra electron in the valence band or smears the charge uniformly over space. In some cases, as the case of metallic Cu, introducing half a core-hole (i.e., the core level half occupied with an electron) fits better the experimental ELNES than the full core-hole approximation.<sup>17</sup> The half-hole method is consistent with the Slater’s transition state theory and reproduces more accurately the binding energies for EELS thresholds.<sup>18</sup> All those approaches require much computation time because the self-consistent calculations should be performed in the extended unit cell (supercell) in order to exclude nonphysical interactions between the neighboring holes. In practice, the choice

for one particular flavor of the core hole is most often made by comparison with experimental spectra.

In the present work we will estimate the effect of the core hole on the intensity scale of the calculated cross sections rather than on the changes in the ELNES, which are averaged when integrating over the energy window. Figure 6(a) demonstrates that account for the core hole affects significantly the intensity scale of the O  $K$  edge of TiO<sub>2</sub> rutile and, to a smaller extent, the  $L_{2,3}$  one [not shown in Fig. 6(a)]. However, as seen from Fig. 6(b), the ratio between the  $L_3$  integrated cross sections in TiO<sub>2</sub> rutile and TiO is quite similar to that in the ground state calculations [Fig. 4(d)]. The major effect of the core hole is introducing an intensity scaling factor, which is almost independent of the chemical environment of an atom.

As seen in Fig. 6(a), the intensity scaling factor depends crucially on the specific method of accounting for the core hole. In the standard full- or half-core hole approximation, both initial core and final states are calculated with a potential perturbed by the core hole in the one-electron formula (2). Considering the many-body problem Stern and Rehr<sup>19</sup> showed that this approach is reasonable for transition metals with almost empty  $d$ -band, as in the case of Ti. Note, however, that formula (9) in Ref. 19 includes the core orbital in the *unperturbed* potential. Contrary to the standard core hole calculations, taking the initial states with the ground state potential and final states with the perturbed one (the “mixed” approach) results in an increase of the intensity scaling factor

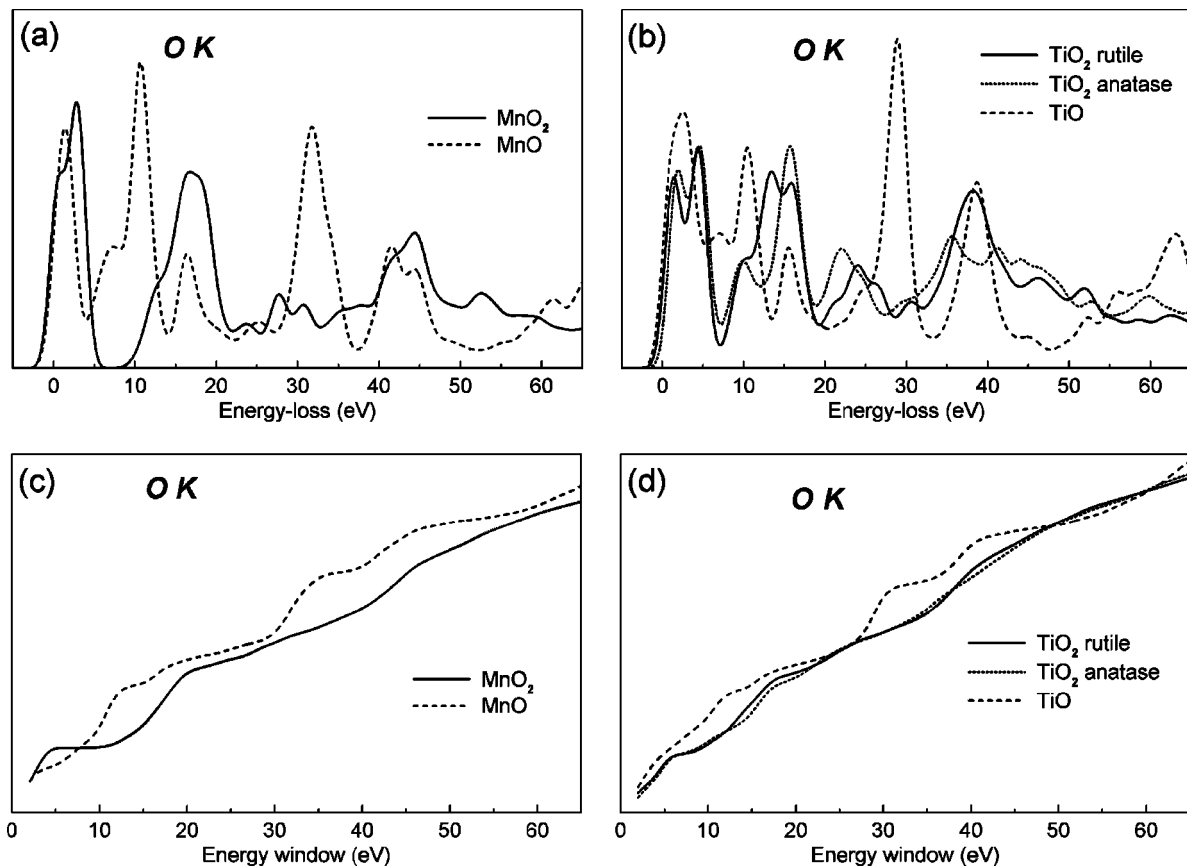


FIG. 5. LAPW ground state calculated (a,b) ELNES and (c,d) integrated cross sections of the O  $K$  edge in (a,c) the Mn oxides and (b,d) the Ti oxides.

[Fig. 6(a), upper curve] while the ELNES is almost unchanged comparing with the standard approaches. For metals with a half filled  $d$ -band, as Mn, the one electron picture is less confident as multielectron excitations might be not negligible.<sup>19</sup>

#### E. Calculating ratio between O $K$ and Me $L_{2,3}$ cross sections

The comparison between theoretical and experimental cross sections can be made by relating the calculated intensities of Me (metal)  $L_{2,3}$  to the O  $K$  edges. One difficulty is the influence of the core hole discussed in the previous section. Although the effect of the core hole seems to be independent on the chemical environment of a given atom, it might result in different intensity scales when *different* atoms are compared. As the intensity scaling factor is different for  $K$  and  $L_{2,3}$  edges, the choice of the particular method for accounting for the core-hole would affect the O to Me ratio. The best fit with the experimental Me  $L_{2,3}$  to O  $K$  ratio is obtained when the final states are calculated with a potential perturbed by a full core hole while the initial states are taken from the ground state. The calculations reveal that this “mixed” approach results in a 25%–30% increase of the O to Me edge ratio when compared with the ground state approximation. In the case of Mn oxides, the “mixed” approach cannot be justified as multielectron effects are expected to be strong;<sup>19</sup> however, as will be seen further, a fit with experiment is surprisingly good in the Mn series.

Another difficulty arises when summing the total  $L_{2,3}$  edge from the partial  $L_3$  and  $L_2$  contributions. As a LAPW method is a one-electron approach, it predicts the statistical (2:1) branching ratio between the intensities of  $L_3$  and  $L_2$  edges. In reality, the experimental ratio is always less than 1.0 for the Ti  $L_{2,3}$  edges and more than 2.0 for the Mn ones. Only approaches involving explicitly many-body effects, for instance the time-dependent local density approximation,<sup>20</sup> can reproduce the correct branching ratios. The many-body effects redistribute intensity between the  $L_3$  and  $L_2$  edges but are unlikely to affect the integral over the total ( $L_3+L_2$ ) cross section. This was demonstrated by the atomic multiplet theory—the simplest method accounting for many-body effects, which provides realistic branching ratios in transition metals<sup>21,22</sup> but still results in the integrated ( $L_3+L_2$ ) cross section exactly equal to that in the one-electron description.<sup>23,24</sup> Since the present calculations are kept within the one-electron picture, the branching ratio of 2:1 might cause errors at energy-losses comparable with the value of the  $L_3-L_2$  splitting. Fortunately, in the case of Ti, the error is negligible because of the small (5.8 eV) splitting value while the most interesting energy region for the study of charge transfer is 10–20 eV. In the case of Mn, the splitting is about 10.5 eV but the experimental branching ratio is not much different from the statistical value and again the one-electron description is reasonable.

Figure 7 shows the ratios between the O  $K$  and Me  $L_{2,3}$  edges intensities calculated by LAPW within the “mixed”

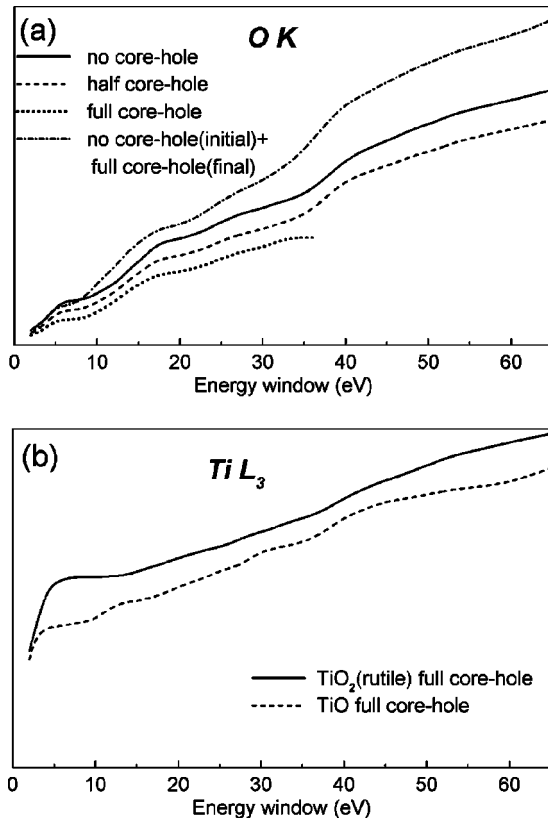


FIG. 6. Effect of the core hole on the LAPW (a) O *K* integrated cross sections in TiO<sub>2</sub> rutile calculated with different approaches and (b) the Ti *L*<sub>3</sub> integrated cross sections in rutile and TiO calculated in the standard full core hole approximation.

core hole approach and measured experimentally. Unlike Table I, the nominal ratio between the numbers of oxygen and metal atoms is not accounted for, thus this plot is expected to reflect the stoichiometry of oxides. “Mixed” core hole LAPW calculations reproduce adequately the experimental O/Me ratio at small energy windows while slightly underestimating it when increasing the window above 40–50 eV. Apparently this relates with the underestimation of continuum states in the O *K* edge as mentioned earlier [see Fig. 3(c)]. Figure 7 also displays the calculations in the free-atom approach, which implies the cross sections independent on chemical environment; thus all differences in the intensity ratios relate solely to the different stoichiometry of oxides. The atomic calculations fail completely at small energy windows and predict the wrong direction of change of the ratio with increasing window width. Due to the wrong energy dependence they can be compared with the experiment only at windows larger than 70 eV, where both atomic calculated and experimental ratios become quasi-independent on energy. Note that the experiment fits approximately the LAPW calculations at low energy-losses and the atomic calculations in the large energy windows, which confirms the complementarity of these two approaches discussed in Sec. III B.

To elucidate the changes in the cross sections, the O/Me ratio in the IV valence oxide is divided by that in the II valence ones and plotted in Fig. 8. In the absence of charge

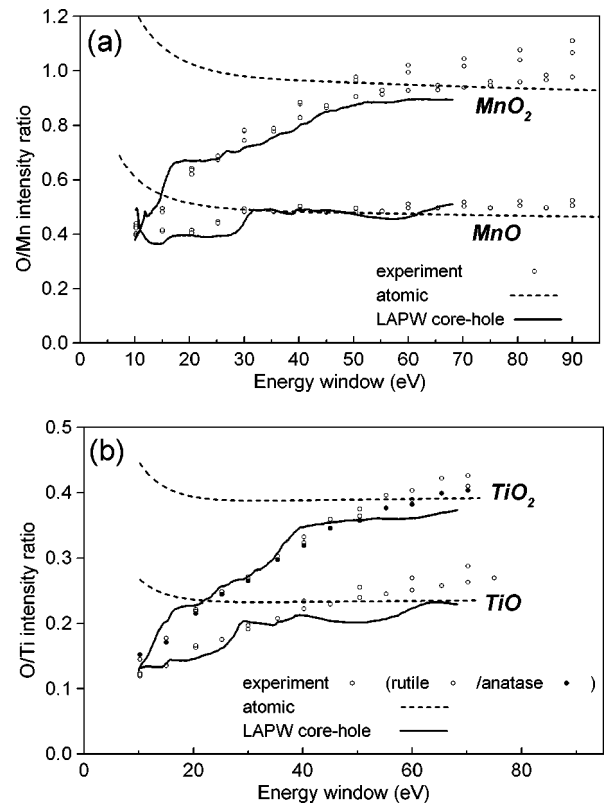


FIG. 7. The ratios between the O *K* and Me *L*<sub>2,3</sub> edge intensities along with the theoretical values calculated by LAPW (“mixed” core-hole approach) and by an atomic model.

transfer, the result must only reflect the stoichiometry of the compared oxides regardless of the energy window used. That should be 2.0 for MnO–MnO<sub>2</sub> series and 1.66 for TiO<sub>1.2</sub>–TiO<sub>2</sub> series. The ELNES variation might affect the result although its effect is expected to be random and quickly damping with increasing energy window. However, Fig. 8 reveals that in both the Mn and Ti oxides series, the experimental curves systematically deviate to lower values from 2.0 and 1.66 expected respectively for Mn and Ti. The deviation is quite pronounced in the 10–20 eV windows and dampens out with increasing energy window. Both the ground state and core-hole LAPW calculations reproduce this trend and agree quite reasonably with experimental numbers. As seen from Figs. 4(c) and 4(d), the effect originates mainly from the changes in the metal *L*<sub>3</sub> and *L*<sub>2</sub> cross sections in the 10–15 eV windows, which extends to 10–20 eV when accounting for the *L*<sub>3</sub>–*L*<sub>2</sub> splitting. It should be noted that, although the ground state approach underestimates the O to Me edge ratio, the errors are cancelled out by dividing the two O/Me ratios by each other and the results of ground state and “mixed” core hole calculations look comparable in Fig. 8.

#### IV. DISCUSSION

Prevalence of the continuum states at high energy makes the integrated cross section independent on chemical environment of a given element. This property is essential for the

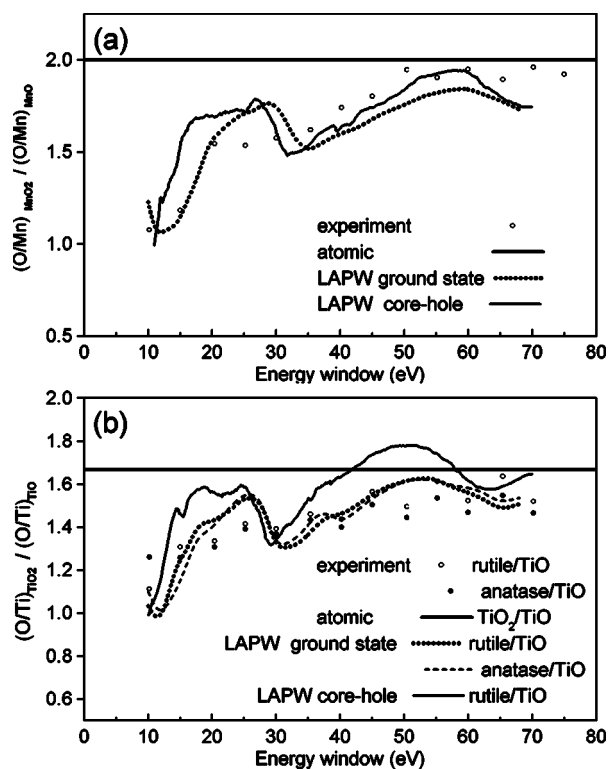


FIG. 8. The experimental and LAPW (ground state and “mixed” core-hole approaches) calculated O/Me ratio in the IV valence oxide divided by that in the II valence oxide in (a) manganese and (b) titanium series, revealing a charge transfer from a metal atom to an oxygen atom during progressing oxidation from the II valence to the IV valence oxide.

elemental analysis with EELS when the cross sections are calculated in the atomic model. However, as seen from Table I and Fig. 7, the assumption of an environment-independent cross section is approximately correct only when large energy windows are used. In many cases, e.g., in the case of energy-filtered transmission electron microscopy (EFTEM), smaller windows are employed to maximize the signal-to-noise ratio. Still, the elemental analysis is possible provided that the integrated cross sections are calculated by LAPW with several precautions outlined in Secs. III B–III E and the Appendix. These LAPW calculations allow us to avoid complicated (and in many cases impossible) experimental measurements of high precision. As seen from Fig. 7, at high energies, LAPW is consistent with the atomic calculations, i.e., a smooth connection between these two approaches is obtained.

It should be clearly realized that the charge transfer might have a strong impact on the EELS cross sections in the energy region close to the threshold. As a consequence, the Me cross section  $\sigma_{\text{Me}}$  in formula (1) is biased by the valence state and the Me integrated intensity  $I_{\text{Me}}$  is not proportional to the numbers of Me atoms  $x$  anymore. Fortunately, the present results suggest that the charge transfer effect roughly correlates with the formal valence of the oxide as seen from Figs. 3(c) and 3(d). In metals, the integrated cross sections follow very similar curves almost independently of the specific chemical environment and show no noticeable charge

TABLE II. MTR dependence of the Ti  $L_{2,3}$  cross section in hcp Ti.

Muffin tin radius (a.u.)	Extra localized orbitals	Energy window		
		20 eV	40 eV	70 eV
1.4	No	88.14	118.58	155.12
2.0	No	89.31	115.03	136.84
2.4	No	87.54	107.56	122.41
1.4	Yes	88.24	119.37	159.79
2.0	Yes	89.90	121.04	160.34
2.4	Yes	89.85	120.86	159.39

transfer, which supports the concept of EELS local charge neutrality in metallic systems.<sup>25</sup> Taking into account these regularities, the relationship between the composition and the O  $K$ /Me  $L_{2,3}$  intensity ratio can be interpolated for any Me by calculating few reference oxides in the given Me-O system. Furthermore, as seen from Fig. 8, the general trends of changing the cross sections with valence are similar for different oxides families. In principle, Fig. 8, which characterizes the charge transfer between II and IV valence oxides, can be utilized as a basis for parametrization of the cross section vs the valence state.

## V. CONCLUSIONS

The electron charge transferred from metal to oxygen atom in the course of oxidation affects noticeably the experimental EELS integrated cross section in Mn and Ti oxides. The charge transfer effect is most pronounced at 10–20 eV above the threshold and fades with increasing energy-loss due to the increasing contribution of continuum states.

The LAPW method can successfully calculate the contribution of bound states in the EELS integrated cross section including the effect of the charge transfer. The resulted integral cross section is mainly controlled by the formal valence rather than the specific ELNES of the compound. The calculated integrated cross sections are in a good agreement with the experimental ones. Continuum states are less successfully reproduced by LAPW and simpler atomic calculations are still more efficient there.

## ACKNOWLEDGMENTS

This work is supported by a GOA project of the University of Antwerp entitled “Characterization of nano-structures by means of advanced electron energy spectroscopy and filtering.” Useful comments by Jo Verbeeck and John T. Titantah are acknowledged.

## APPENDIX: IMPORTANT PARAMETERS IN LAPW CALCULATION OF EELS INTEGRATED CROSS SECTION

A crucial parameter in the LAPW calculations is the muffin tin radius (MTR). Since the muffin tin is an entirely technical concept, while the cross section is a physical value, the latter should not depend on MTR. From formula (2) it is seen

TABLE III. Convergence of the integrated Ni  $L_{2,3}$  cross section in TiNi with respect to density of mesh for integration over scattering vector  $\mathbf{q}$ .

Energy window	1 point	8 points	27 points	64 points	125 points
10 eV	9.04	11.84	12.50	12.71	12.72
20 eV	13.45	17.57	18.53	18.83	18.84
30 eV	16.00	20.88	22.00	22.35	22.36

that the cross section is essentially an overlap integral of initial and final state wave function. The strong localization of the core orbital provides a natural radial cutoff for calculation of this integral. Since, for computational reasons, the muffin tin has always to be larger than the core orbitals, artificial dependence of the cross section on MTR is not expected.

However, when using the default LAPW basis we do observe strong MTR-dependence of the high energy part of the spectrum (energy windows 40 eV and higher), resulting in

lower integrated cross sections for larger MTR (see Table II). The default LAPW basis set is intended for the description of bound states only, while the continuum states are less well described in large MTR calculation yielding a lower DOS at high energy. The description of the continuum states by the muffin tin basis is getting worse as one goes away from the nucleus. As seen from Table II, the addition of local orbitals to a basis set raises the continuum DOS for large muffin tin spheres and makes the EELS cross section quasi-independent of MTR.

Secondly, the collection and convergence angles have to be explicitly taken into account to simulate experimental EELS cross sections. The collection angle is accounted for by numerical integration over the distribution of allowed scattering vectors. As seen from Table III, this integration is converged by using a sufficiently dense mesh of  $\mathbf{q}$ -vectors. In the present work, a mesh of 75 points was chosen for all calculations. The influence of convergence angle is minor at the experimental conditions used, and these small corrections were accounted for empirically after Kohl *et al.*<sup>15</sup>

<sup>1</sup>D. H. Pearson, C. C. Ahn, and B. Fultz, Phys. Rev. B **47**, 8471 (1993).

<sup>2</sup>H. Kurata and C. Colliex, Phys. Rev. B **48**, 2102 (1993).

<sup>3</sup>D. A. Muller, D. J. Singh, and J. Silcox, Phys. Rev. B **57**, 8181 (1998).

<sup>4</sup>Y. Murakami, D. Shindo, K. Otsuka, and T. Oikawa, J. Electron Microsc. **47**, 301 (1998).

<sup>5</sup>P. L. Potapov, S. E. Kulkova, D. Schryvers, and J. Verbeeck, Phys. Rev. B **64**, 184110 (2001).

<sup>6</sup>R. D. Leapman, L. A. Grunes, and P. L. Fejes, Phys. Rev. B **26**, 614 (1982).

<sup>7</sup>R. D. Leapman, P. Rez, and D. F. Mayers, J. Chem. Phys. **72**, 1232 (1980).

<sup>8</sup>C. C. Ahn and P. Rez, Ultramicroscopy **17**, 105 (1985).

<sup>9</sup>M. Nelhiebel, P.-H. Louf, P. Schattschneider, P. Blaha, K. Schwarz, and B. Jouffrey, Phys. Rev. B **59**, 12807 (1999).

<sup>10</sup>C. Hébert-Souche, P.-H. Louf, P. Blaha, M. Nelhiebel, J. Luitz, P. Schattschneider, K. Schwarz, and B. Jouffrey, Ultramicroscopy **83**, 9 (2000).

<sup>11</sup>S. Andersson, B. Collen, U. Kuylenstierna, and A. Magneli, Acta Chem. Scand. (1947-1973) **11**, 1641 (1953).

<sup>12</sup>D. Watanabe, J. R. Castles, A. Jostsons, and A. S. Malin, Acta Crystallogr. **23**, 37 (1967).

<sup>13</sup>R. F. Egerton, *Electron Energy-Loss Spectroscopy in the Electron Microscope*, 2nd ed. (Plenum Press, New York, 1996).

<sup>14</sup>P. Blaha, K. Schwarz, G. K. H. Madsen, D. Kvasnicka, and J. Luitz, WIEN2K, *An Augmented Plane Wave + Local Orbitals Program for Calculating Crystal Properties*, ISBN 3-9501031-1-2 (Technical Universität Wien, Austria, 2001).

<sup>15</sup>H. Kohl, Ultramicroscopy **16**, 265 (1985).

<sup>16</sup>J. E. Müller, O. Epsen, and J. W. Wilkins, Solid State Commun. **42**, 365 (1982).

<sup>17</sup>J. Luitz, M. Mayer, C. Hébert, P. Schattschneider, P. Blaha, K. Schwarz, and B. Jouffrey, Eur. Phys. J. B **21**, 363 (2001).

<sup>18</sup>A. T. Paxton, M. van Schilfgaarde, M. MacKenzie, and A. J. Craven, J. Phys.: Condens. Matter **12**, 729 (2000).

<sup>19</sup>E. A. Stern and J. J. Rehr, Phys. Rev. B **27**, 3351 (1983).

<sup>20</sup>A. L. Ankudinov, A. I. Nesvizhskii, and J. J. Rehr, Phys. Rev. B **67**, 115120 (2003).

<sup>21</sup>W. G. Waddington, P. Rez, I. P. Grant, and C. J. Humphreys, Phys. Rev. B **34**, 1467 (1986).

<sup>22</sup>B. T. Thole and G. van der Laan, Phys. Rev. B **38**, 3158 (1988).

<sup>23</sup>F. M. F. de Groot, Z. W. Hu, M. F. Lopez, G. Kaindi, F. Guillot, and M. Tronc, J. Chem. Phys. **101**, 6570 (1994).

<sup>24</sup>F. M. F. de Groot (private communication, 2003).

<sup>25</sup>D. A. Muller, Phys. Rev. B **58**, 5989 (1998).